CHAPTER -4

Work Hardening Behaviour of Inconel 617 Alloy

4.1 Introduction

Alloys with low stacking fault energy (SFE) exhibit deviation from the Hollomon relationship [41] in the true stress and true plastic strain curves, in the region of low plastic strain due to change in the deformation behaviour during plastic deformation. Ni-based superalloys usually exhibit this type of deviation. Different models have been proposed to characterize the plastic flow and work hardening behaviour of these materials [42-45]. Work hardening behaviour of the stainless steels and other ferrous materials has been the subject of research by several investigators. However, no systematic investigation has been carried out on work hardening behaviour of the Inconel 617 alloy. Application of the Inconel 617 alloy as boiler tubes and super-heater tubes requires understanding of its microstructural stability and its deformation behaviour under tensile, creep, and cyclic loading at the service temperature. The mechanical properties of such materials are governed by their grain size, dislocation density as well as the type, volume fraction and distribution of the strengthening precipitates. Hence, the present investigation is aimed at studying work hardening behaviour of the Inconel 617 alloy under tensile loading at room temperature and 700^{o}C in various conditions. The present chapter discusses the effect of different treatments on the evolution of microstructure and work hardening behaviour of the Inconel 617 alloy at room temperature (RT) and service temperature (700^{o}C) of the boiler tubes used in the A-USC power plants.

Several studies have been carried out in solution treated (SQ) condition of Inconel 617 alloy [12, 33, 34, 40]. Hosier and Tillak [13], Mankins et al. [12], Kirchhofer et al. [14], Wu et al. [15], Kimball et al. [48] have studied the aging heat treatment and characterized precipitation behaviour of the alloy. They observed precipitation of carbides after aging at different temperatures for varying durations and

found that hardness was increased with increase in the duration of aging. Mo et al. [49] analyzed the influence of aging temperatures 900^{o}C and 1000^{o}C for longer durations on properties and found that mechanical properties were improved from aging up to 3000 h at both the temperatures. Jo et al. [52] observed coarsening of carbides and marginal change in mechanical properties of the Inconel 617 alloy from the long exposure up to 1000 h at 1050^{o}C. However, studies which focus on comparison of work hardening behaviour of the Inconel 617 alloy after subjecting it to different conditions such as solution annealing, aging treatment for short durations and cold working are lacking which necessitated the in-depth study taken up in the present chapter.

4.2 Methodology

Tensile tests were performed using cylindrical specimens of 15.5mm gauge length and 4.5mm gauge diameter. The length and diameter of the head portion was 5.3mm and 7.1mm respectively and the shoulder radius was 0.8 mm. Tensile tests were carried out at RT and 700°C, at a strain rate of $5x10^{-3}$ s^{-1} using Instron^{TM} universal testing machine (Model: 4206). Tests matrix for studying work hardening behaviour is given in Table 4.1

Table 4.1 Designations of the Inconel 617 Alloy used to Study Work Hardening Behaviour.

S. No.	Condition	Designation
1.	Solution treated at 1175^{o}C for 40 minutes and water quenched	SQ
2.	Solution treated at 1175^{o}C for 40 minutes, water quenched and aged at 850^{o}C for 100h	SQ-AG1
3.	Solution treated at 1175^{o}C for 40 minutes, water quenched and aged at 850^{o}C for 500h	SQ-AG2
4.	Solution treated at 1175^{o}C for 40 minutes, water quenched and cold rolled (40% reduction)	SQ-CW

Various relationships for characterizing work hardening behaviour, proposed by Hollomon, Ludwigson, Ludwik, Swift and Voce [41-45], were applied to analyze work hardening behaviour of the Inconel 617 alloy in the four different conditions. These relationships are described below.

Hollomon equation: $\sigma = K\varepsilon^{n}$ ---------- (4.1)

where, σ: true stress, ε: true plastic strain, K: strength co-efficient and n: strain hardening exponent.

Ludwigson equation: $\sigma = K\varepsilon^{n} + \exp(K_1 + n_1\varepsilon)$ ---------- (4.2)

K_1, n_1: additional constants

Ludwik equation: $\sigma = \sigma_o + K\varepsilon^{n}$ ---------- (4.3)

Where σ_o: yield stress

Swift equation: $\sigma = K(\varepsilon_o + \varepsilon)^{n}$ ---------- (4.4)

Where ε_o: pre strain in the material.

Voce equation: $\sigma = \sigma_s - (\sigma_s - \sigma_I)\exp(n\varepsilon)$ ---------- (4.5)

σ_s: saturation stress and σ_I: true plastic stress (yield).

4.3 Microstructure in Different Conditions

Microstructure of the Inconel 617 alloy in the AR condition and SQ condition is shown in Fig. 3.1 and 3.2 respectively in the previous chapter (section 3.3) In AR condition, the microstructure comprises of mostly equiaxed grains of small size and some elongated grains, with large number of precipitates distributed throughout the matrix and the solution treated alloy (SQ) shows single phase matrix of the austenite without the precipitates and annealing twins in some grains. Figs. 4.1a and b show the microstructure in the SQ-AG1 condition, almost similar to that of the SQ condition, along with the presence of Cr rich carbides. Fig. 4.1c confirms the presence of Cr rich

carbides through EDS analysis. Similar microstructure is observed also in the SQ-AG2 condition (Fig. 4.2a and b) except that there is increase in the number of precipitates and annealing twins. EDS analysis shown in Fig. 4.2c confirms the particles shown by arrow as Mo and Cr rich carbides. Similar observations have been made also earlier in the aged samples [14, 54].

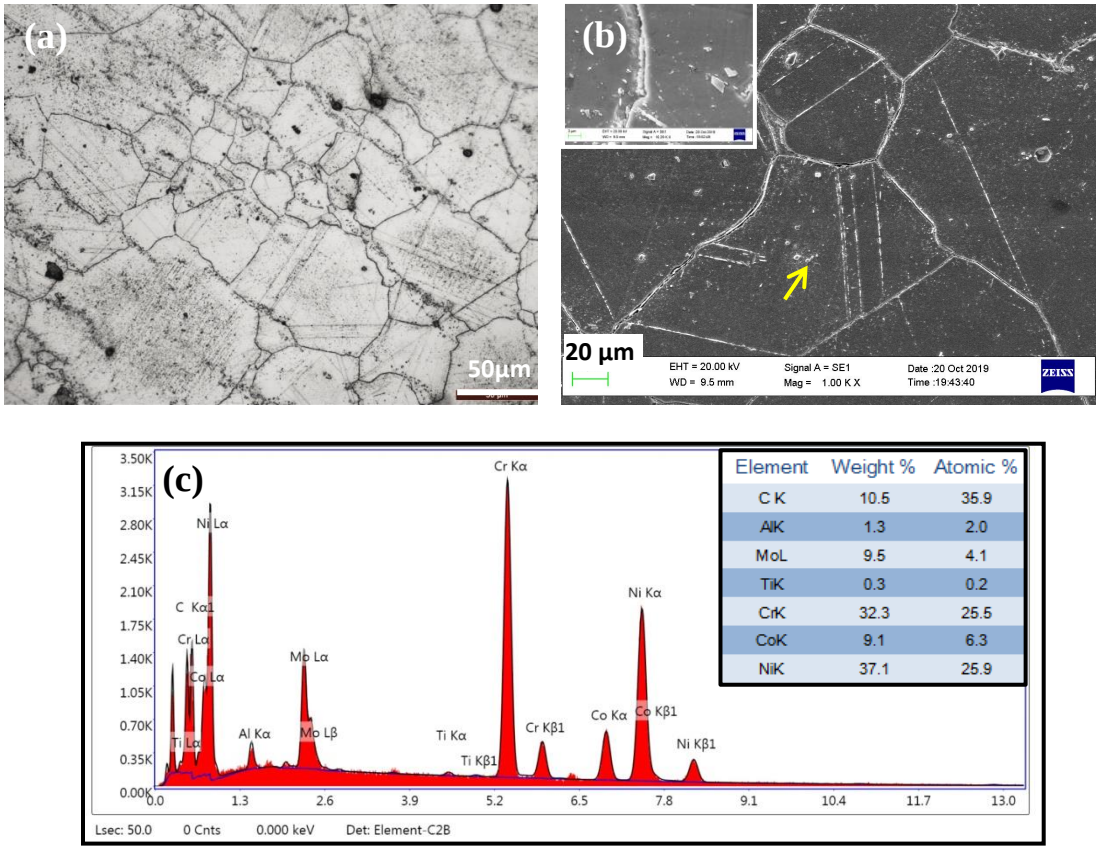

Fig. 4.1: Microstructure of Inconel 617 alloy in SQ-AG1 (100 h) condition: (a) Optical micrograph indicating single phase (γ) matrix with fine precipitates within grains and grain boundaries (b) SEM micrograph showing precipitates of Cr rich carbides (arrow) (c) EDS analysis for Cr rich carbides.

Fig. 4.3 shows microstructure of this alloy in the cold worked condition with elongated grains and carbides aligned as bands. Also cracks were observed in the matrix due to de-cohesion of the carbide particles from the grain boundaries (as shown in the inset image). The microstructure of the cold worked sample is in line with that observed by Wright et al. [101]. XRD analysis of all the five samples in the different conditions is

shown in Fig. 4.4, with distinct peaks of the face centered cubic (*fcc*) matrix of γ in SQ condition and peaks of the precipitates in the AR and SQ-AG2 conditions.

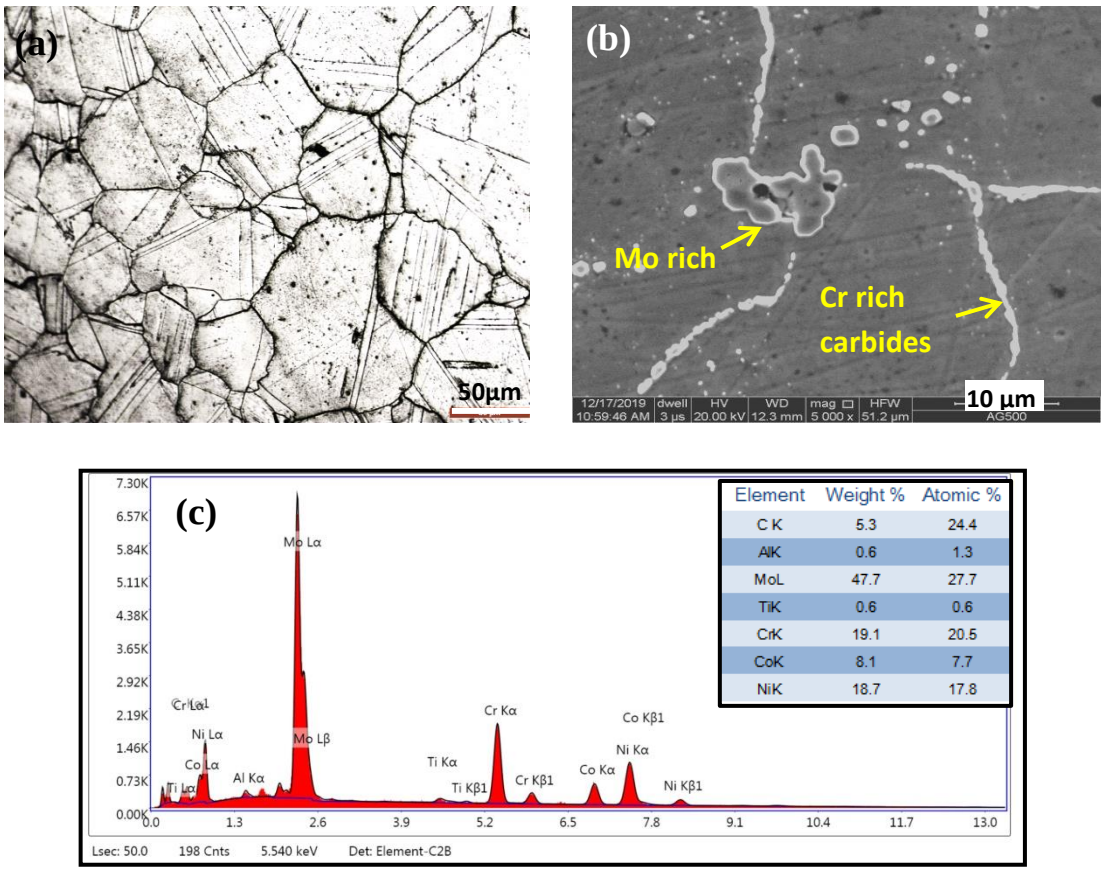

Fig. 4.2: Microstructure of the Inconel 617 alloy in SQ-AG2 (500 h) condition: (a) Optical micrograph showing single phase (γ) matrix with fine precipitates, along with annealing twins (b) SEM micrograph showing Mo rich and Cr rich carbides (c) EDS analysis of Mo and Cr rich carbides.

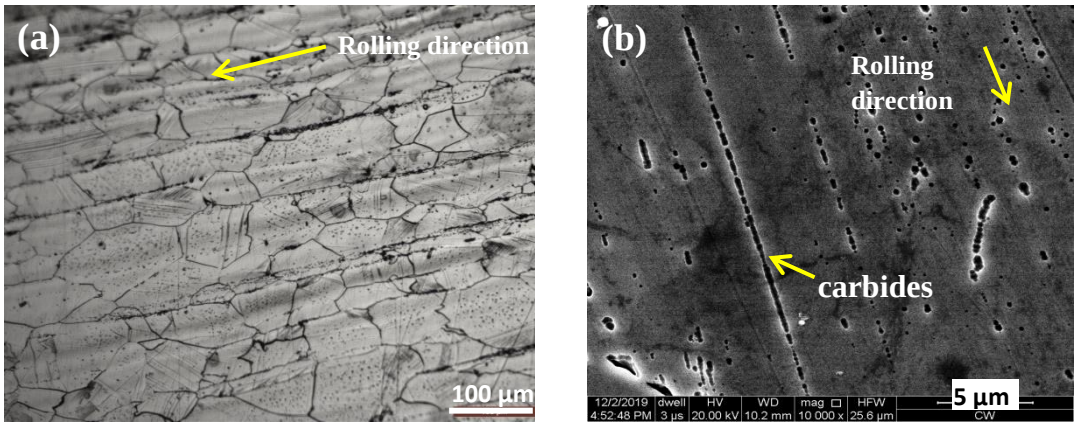

Fig. 4.3: Microstructure of Inconel 617 alloy after solution annealing at 1175°C for 40 minutes and cold working (40%) (SQ-CW): (a) Optical micrograph indicating single phase (γ) matrix, with elongated grains and carbides aligned in rolling direction as bands (b) SEM micrograph showing magnified view of carbide bands.

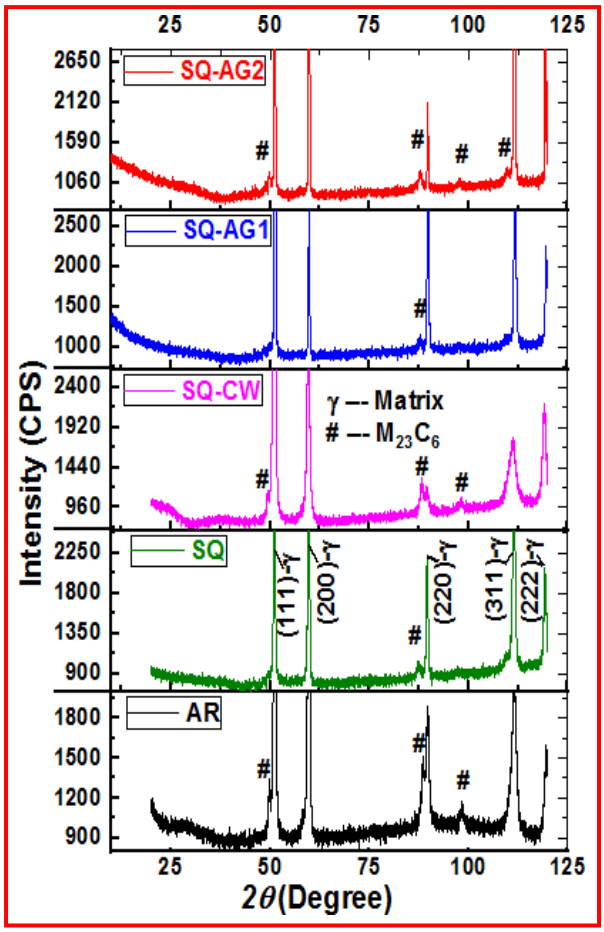

Fig. 4.4: XRD analysis of the Inconel 617 alloy in different conditions.

4.4 Engineering Stress-Strain Behaviour

Figs. 4.5a and 4.5b shows the engineering stress – plastic strain curves of the Inconel 617 alloy in the four different conditions, tested at RT and 700^{o}C respectively. A typical ductile behaviour was observed in the three conditions (SQ, SQ-AG1 and SQ-AG2) whereas very low ductility was observed in the SQ-CW condition. Table 4.2 shows various tensile properties of the Inconel 617 alloy in different conditions, at RT and 700^{o}C. At RT, 0.2% offset yield strength (YS) is highest in the SQ-CW condition whereas it is much lower in the other three conditions (SQ, SQ-AG1 and SQ-AG2). The ultimate tensile strength (UTS) values also follow the same trend. However, the strength parameters of the aged samples were higher at RT as compared to that of the SQ

condition, though the increase in the duration of aging from 100h to 500h did not have any significant effect on the strength of the aged samples. The ductility values, in particular the uniform elongation (e_{pu}) was lowest (3.7%) in the SQ-CW condition. On the other hand, e_{pu} is significantly higher in the other three conditions. The total elongation i.e. elongation to fracture (e_{pf}) in the SQ condition is much higher than in the other conditions, at room temperature. It may be seen that while there is so much variation in the e_u and e_f, there is not much difference in the reduction in area.

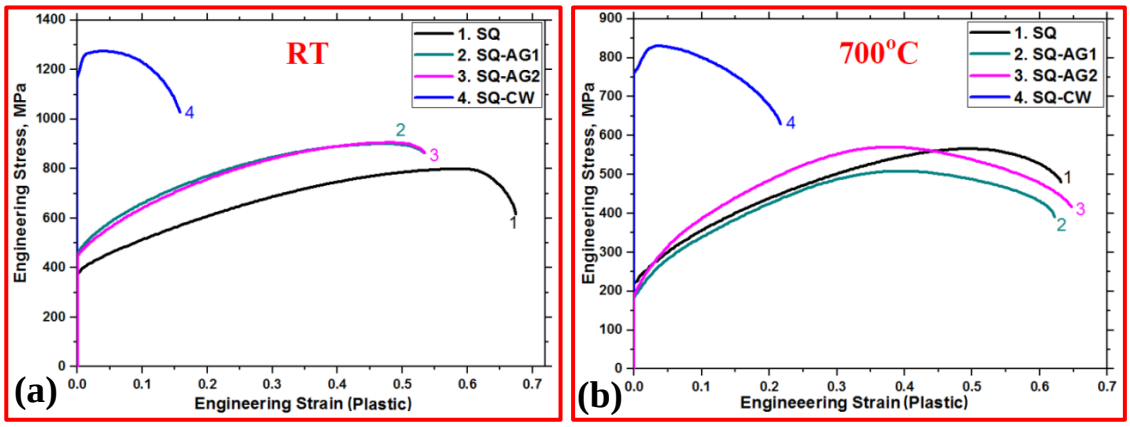

Fig. 4.5: Engineering stress–engineering strain (plastic) curves of the Inconel 617 alloy in different conditions tested at a strain rate of $5x10^{-3}$ s^{-1} at: (a) RT and (b) 700°C.

At 700°C, YS and UTS are highest for the SQ-CW condition. As expected the strength values are higher at room temperature than those at 700°C for all the conditions. It may be seen that the values of e_{pu} for all the four conditions, at 700°C, are lower than the respective values at RT. There is similar trend in the %RA at RT and 700°C. In contrast to these there is increase in the e_{pf} with rise in temperature from RT to 700°C except for the SQ. The degree of work hardening (S_{UTS}/S_{YS}) is higher at 700°C than that at RT for all the four conditions. The degree of work hardening at RT is highest in the SQ and at 700°C it is highest in the SQ-AG2.

Table 4.2: Tensile properties of Inconel 617 alloy at RT and 700°C

Condition	0.2% YS (S_{YS}) MPa	UTS (S_{UTS}) MPa	Uniform elongation (e_{pu}), %	Elongation to fracture (e_{pf}), %	RA %	S_{UTS}/S_{YS}
RT						
SQ	385	805	59.9	67.9	52	2.09
SQ-AG1	457	902	49.1	54.7	59	1.97
SQ-AG2	448	905	49.5	55.2	58	2.02
SQ-CW	1229	1280	3.7	16.5	43	1.04
700°C						
SQ	217	570	51.4	61.8	52	2.60
SQ-AG1	184	512	39.6	62.5	43	2.78
SQ-AG2	192	570	38.3	64.7	44	2.96
SQ-CW	782	833	4.0	22.5	28	1.06

4.5 Work Hardening Behaviour

Fig. 4.6a and b shows double logarithmic plots of the true stress *vs.* true plastic strain for all the conditions of the Inconel 617 alloy tested at RT and 700°C respectively. It clearly shows upward concave shape of the curves for all the conditions except for the SQ-CW at both the temperatures. The work hardening behaviour of the Inconel 617 alloy is analyzed using the five relationships to find out various work hardening parameters. Fig. 4.7 shows true stress- plastic strain curves derived from the different equations referred to above, for all the condition of the sample tested at RT and 700°C. Among all the five relationships, the true stress- true plastic strain curve derived from the Ludwigson relationship has the best fit with the experimental data with high R-square (co-efficient of determination) values and low chi square (χ^2) values.

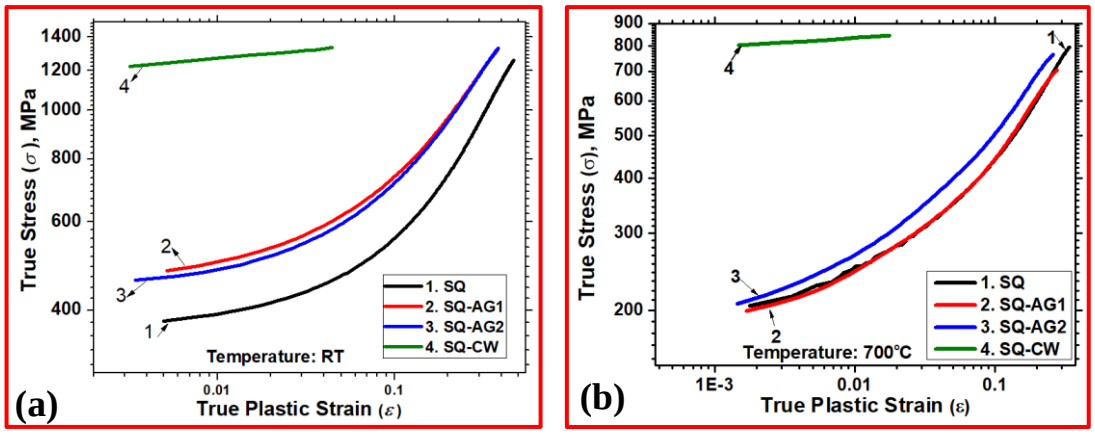

Fig. 4.6: Double logarithmic plots of the true stress *vs.* true plastic strain of the Inconel 617 alloy for all the conditions, tested at: (a) RT and (b) 700°C.

The values of R^2 and χ^2 for different conditions of the alloy using the Ludwigson equation for the data at RT and 700°C are recorded in Table 4.3. The χ^2 values exhibited by the Ludwigson equation are comparatively lower than that obtained by the Hollomon, Ludwik, Swift and Voce equations at both the temperatures, except for the SQ- CW condition at RT, where the Hollomon relation has best fit with low χ^2 value. Table 4.3 shows values of K, n, K_1, n_1 and ε_L (transition strain) derived from the Ludwigson equation for all the conditions of the alloy. Decrease in the value of K and increase in value of n may be seen with increase in the test temperature. In the SQ-CW condition at RT, the values of K and that of n are found to be lowest among the four conditions. It may be observed that there was no significant variation in the value of K_1 with respect to the condition of the alloy at RT. The value of n_1 was higher for the SQ-AG1 and SQ-AG2 conditions compared to that of the SQ condition. It may be seen that the value of n_1 was lowest for the SQ-CW condition. The value of the transition strain (ε_L) is found to lie in the range of 0.10 to 0.17 for all the conditions of this alloy (Table 4.3). The transition strain (ε_L) is more in the SQ condition of the alloy at both the temperatures. The transition strain for the SQ-AG1 and SQ-AG2 conditions decreased

with increase in the test temperature.

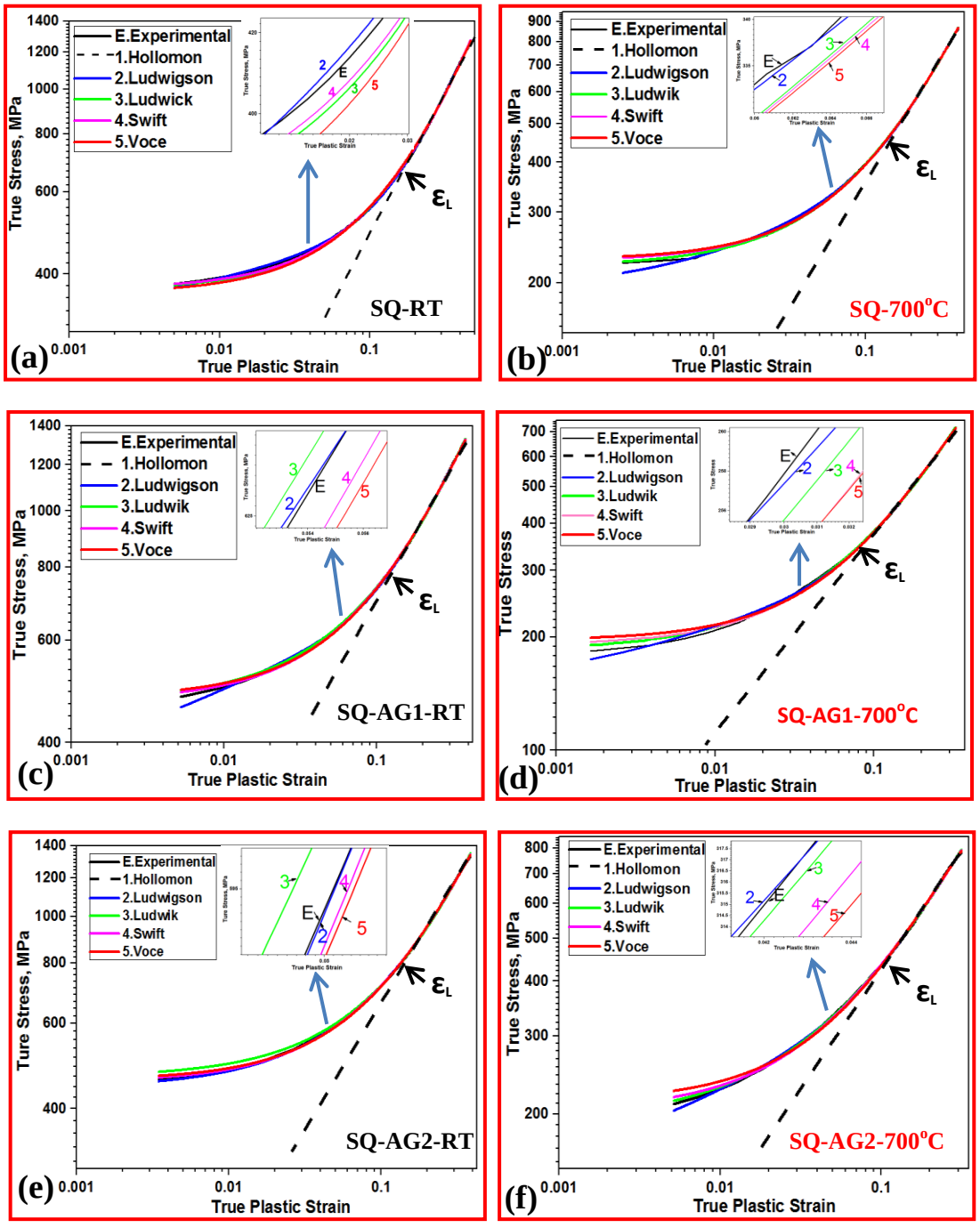

Fig. 4.7: True stress-strain (log-log) curves obtained by using various work hardening relationships and are shown along with the experimental curve: (a) SQ condition at RT (b) SQ condition at 700°C (c) SQ-AG1 condition at RT (d) SQ-AG1 condition at 700°C (e) SQ-AG2 condition at RT and (f) SQ-AG2 condition at 700°C. Magnified view of the curves from the different relationships is shown in the inset.

Table 4.3: Work hardening parameters of Inconel 617 Alloy at RT and 700°C.

Condition	K (MPa)	n	K_1 (MPa)	$-n_1$	ε_L	R^2	χ^2
RT							
SQ	2095	0.633	5.86	14.21	0.212	0.9998	9.3
SQ-AG1	2121	0.490	5.83	19.81	0.150	0.9998	8.8
SQ-AG2	2174	0.514	5.86	20.48	0.170	0.9996	15.3
SQ-CW	1481	0.032	--	--	--	0.9972	5.1
700°C							
SQ	1539	0.643	5.24	14.67	0.153	0.9997	8.5
SQ-AG1	1354	0.573	4.96	21.19	0.103	0.9994	14.3
SQ-AG2	1499	0.554	4.85	22.47	0.102	0.9995	9.2
SQ-CW	1848	0.578	--	--	--	--	--

Work hardening behaviour of the present alloy is also characterized by the rate of work hardening (θ) as a function of σ [102-105]. Fig. 4.8 shows the plot of instantaneous θ *vs.* σ for all the conditions, the values are obtained by numerical differentiation of the true stress corresponding to true strain, displaying three stages of θ variation for the SQ, SQ- AG1 and SQ-AG2 conditions. The value of θ decreased with increase in σ at both the temperatures. Drastic fall in the θ in the Stage I (transition stage) is followed by steady state behaviour in the stage II (Fig. 4.8). The end of the stage I indicate the stress corresponding to transition in the deformation behaviour (σ_t). σ_c indicates the end of the stage II. Stage III is softening stage in which θ decreases rapidly but relatively with lesser rate as compared with that of the stage I. Similar trend is followed for all the three conditions at both the temperatures. At RT, the solution treated material showed lower value of θ compared to those of the SQ-AG1 and SQ-AG2.

The values of θ are lower at 700°C compared with those at RT, for all the four conditions. In the SQ-AG2 condition θ is higher compared to those of the SQ and SQ-

AG1 conditions at 700°C. The stress for the appearance of the stage III is also lower at 700°C, in respect of that at RT. For the SQ-CW condition there is only Stage I both at RT as well as 700°C and θ decreased rapidly with increase in the true stress (σ). It may be seen that the behaviour is quite different from the other three conditions (SQ, SQ-AG1 and SQ- AG2) exhibiting three stages.

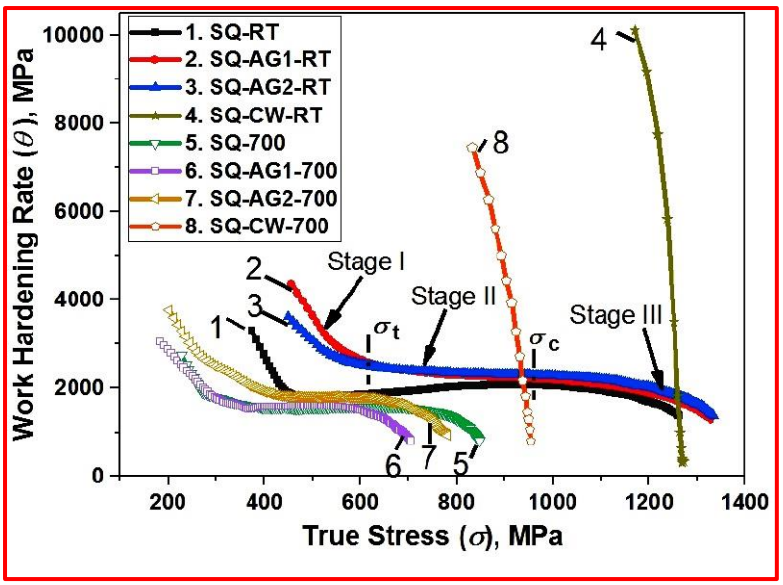

Fig. 4.8: Variation of the work hardening rate (θ) with the true stress (σ) for all the conditions of the Inconel 617 alloy tested at RT and 700°C.

4.6 Deformation Behaviour

Deformation behaviour of the tensile samples tested at RT and 700°C was studied in detail for all the conditions. Deformation behaviour of the SQ sample, tested at RT and 700°C were discussed in Chapter 3 (section 3.10). At RT, Traces of coarse slip bands, and high density of dislocation tangles may be observed within the slip bands. The microstructure of the SQ sample tested at 700°C showed presence of newly formed precipitates (Fig. 3.21a). Interaction of dislocations with precipitates is also evident, showing bowing of dislocation. Fig. 4.9a and b show TEM micrographs of the SQ-AG2 sample tested at RT, precipitates of around 50-70 nm size and non- uniformly

distributed, formed during the initial aging. These precipitates increased the strength only slightly in the aged condition with respect to that of the SQ condition.

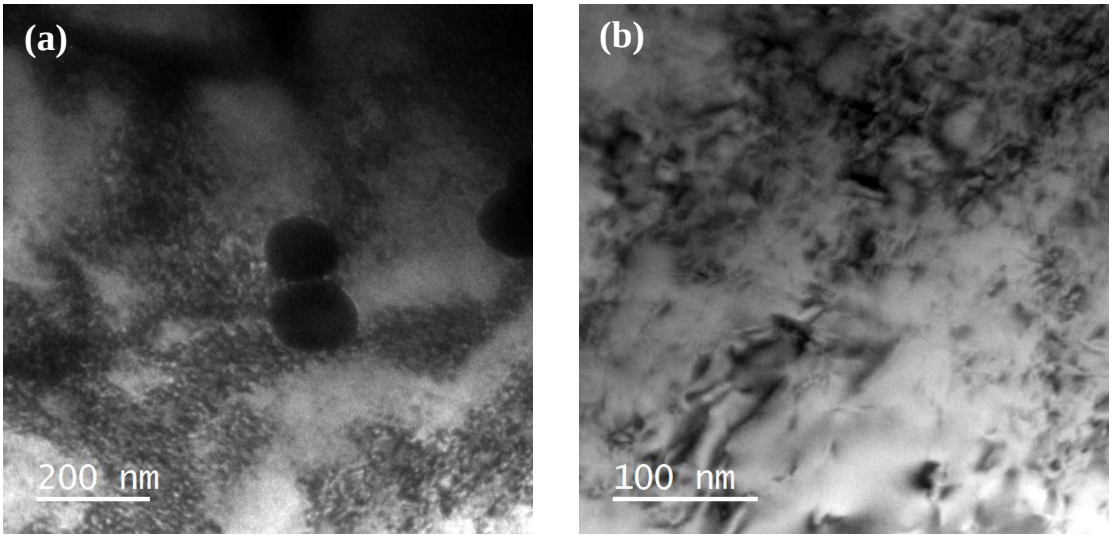

Fig. 4.9: TEM images of tensile tested samples at RT in SQ-AG2 condition showing: (a) forest of dislocations along with carbide particles (formed during aging) (b) dislocation substructure.

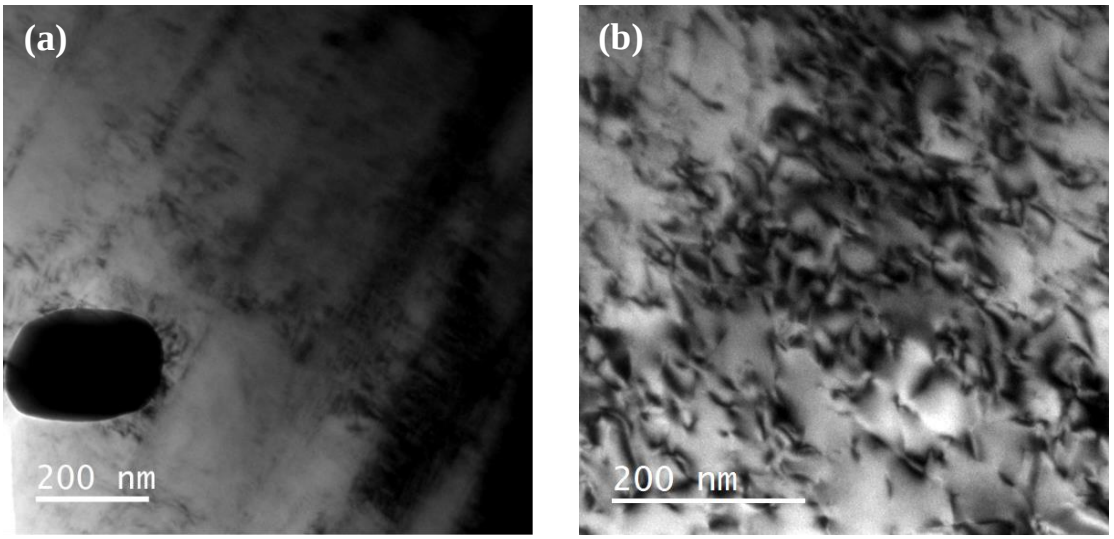

Fig. 4.10: TEM images of tensile tested samples at 700^{o}C in SQ-AG2 condition showing: (a) microtwins present in the structure with carbides formed during aging and (b) interaction of dislocations with precipitates.

At 700^{o}C, (Fig. 4.10) the precipitate-dislocation interaction in the aged condition is observed to be similar to that of the SQ condition. Also twins are observed at this

temperature. The SQ-AG1 and SQ-AG2 samples tested at RT shown deformation behaviour similar to that of SQ except that the presence of precipitates formed during aging in the aged samples which increased the strength only slightly with respect to that of the SQ condition.

Fig. 4.11a shows dislocation pile-up and tangles of dislocations in the SQ-CW sample, tested at RT. Absence of traces of slip bands is a notable feature in this micrograph. Fig. 4.11b shows forest-dislocations, with huge accumulation of dislocations, causing increase in YS and UTS of the alloy. TEM micrograph of the SQ-CW sample, tested at 700^{o}C, is shown in Fig. 4.12a. It shows deformation twins along with newly formed fine precipitates of carbides and γ′. These precipitates are uniformly distributed throughout the matrix. Fig. 4.12b shows interaction of dislocations and precipitates in this condition.

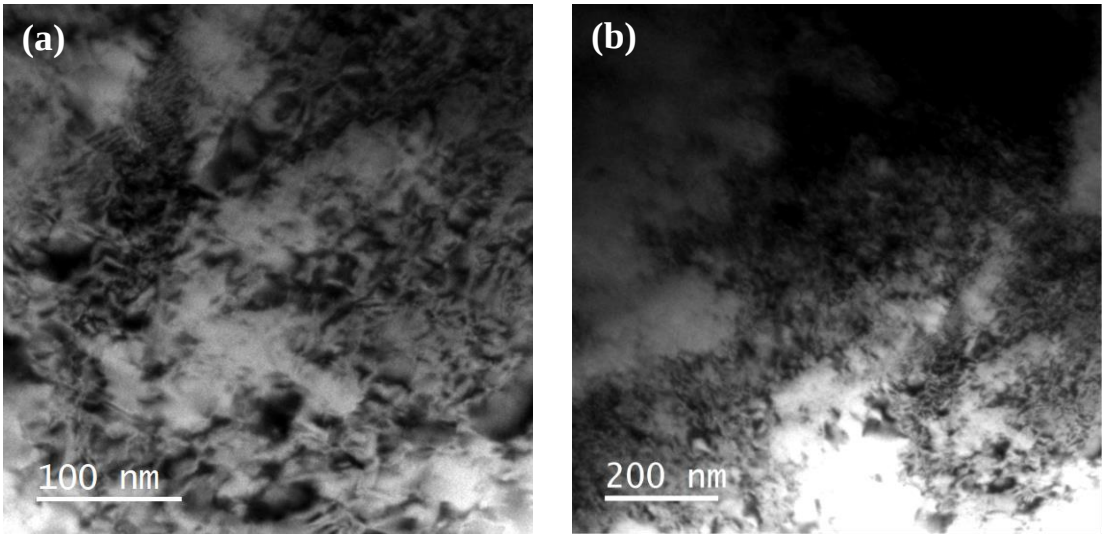

Fig. 4.11: TEM micrographs of tensile tested samples at RT in SQ-CW condition showing: (a) dislocation tangles with precipitates and (b) thick forest of dislocations.

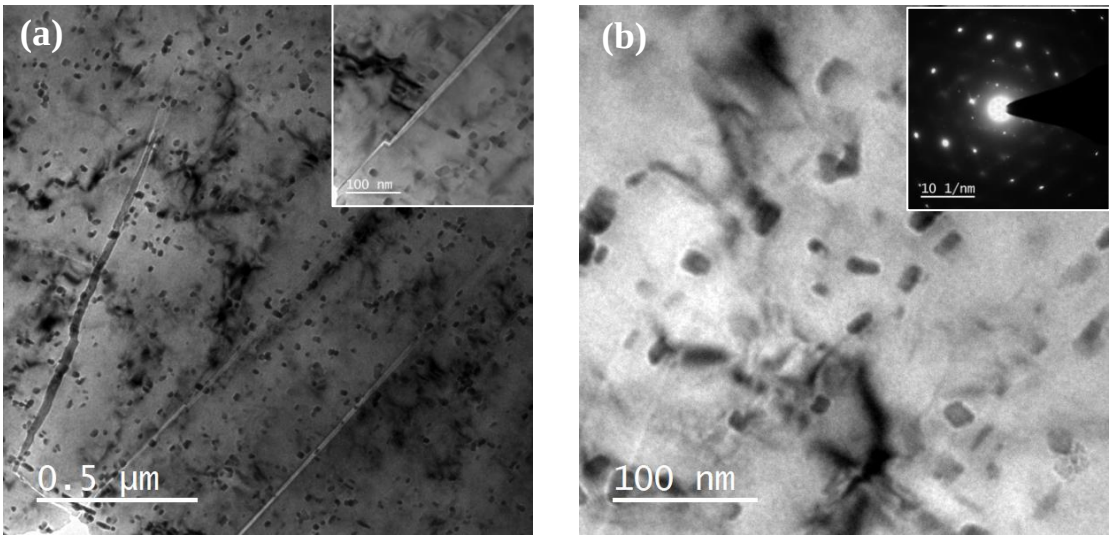

Fig. 4.12: TEM micrographs of tensile tested samples at 700°C in SQ-CW condition showing: (a) deformation twins along with precipitation of carbides ($M_{23}C_6$) and (b) interaction of dislcoations with the precipitates and dislocation tangles.

4.7 Fracture Behaviour

Fracture surfaces of the samples of different conditions, tested at RT and 700°C were characterized using SEM. Fracture surfaces of the SQ sample, tested at RT and 700°C were discussed in section 3.11. In these fractographs, facets and dimples of ≈10-20 μm size were observed. The faceted regions may be seen to be associated with grain boundaries, decorated with coarse carbides. Fractographs of the SQ-AG2 samples for both temperatures are shown in Figs. 4.13 and 4.14 respectively indicate same features as observed in the SQ condition with facets and dimples. Fractographs of the cold worked samples tested at both temperatures (RT & 700°C) are shown in Figs. 4.15 and 4.16 respectively. The region with dimples as well the size of dimples in the SQ-CW sample tested at 700°C is larger compared to that of the SQ- CW sample tested at RT.

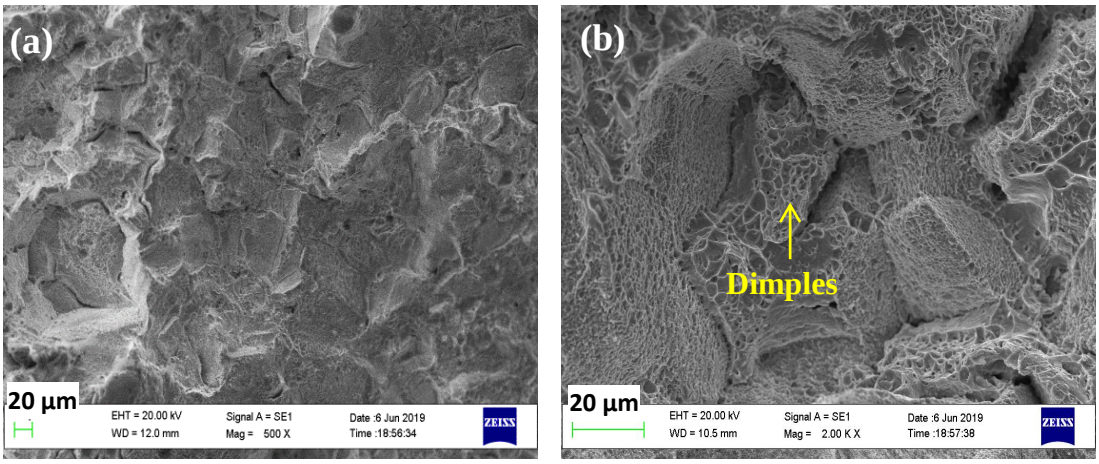

Fig. 4.13: SEM fractographs of tensile tested samples at RT in SQ-AG2 condition showing: (a) dimples throughout the surface and (b) dimples in magnified view.

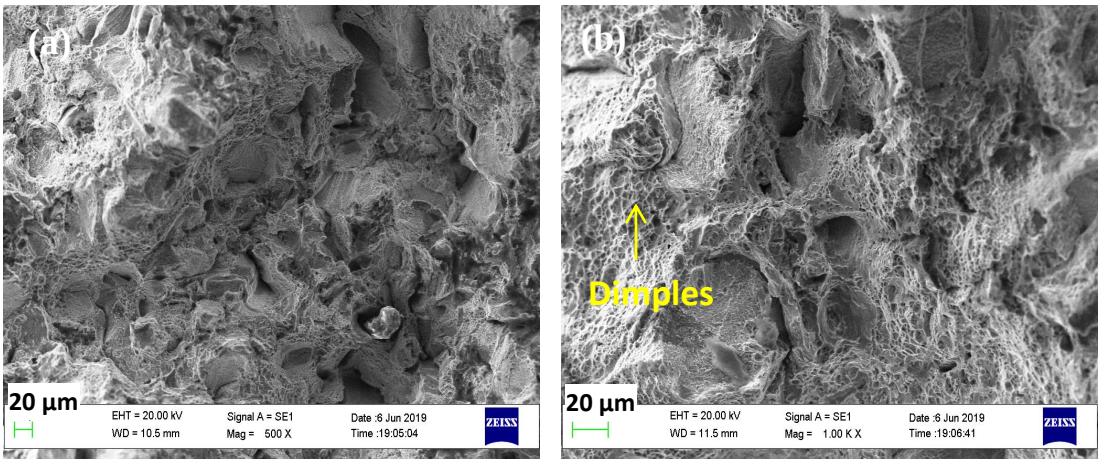

Fig. 4.14: SEM fractographs of tensile tested samples at 700^{o}C in SQ-AG2 condition showing: (a) ductile fracture with facets and (b) magnified view of the facets.

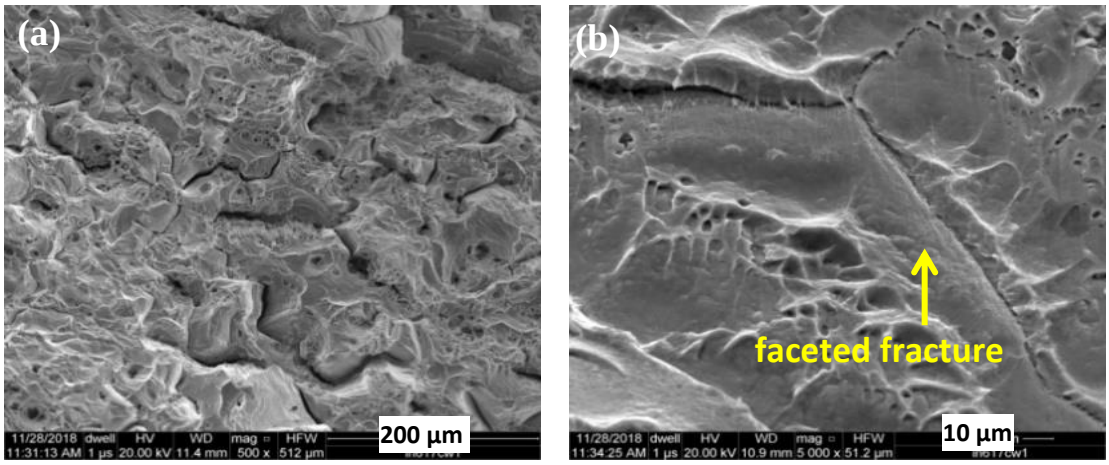

Fig. 4.15: SEM fractographs of tensile tested samples at RT in SQ-CW condition showing: (a) dimples with cleavage facets and (b) magnified view of the facets.

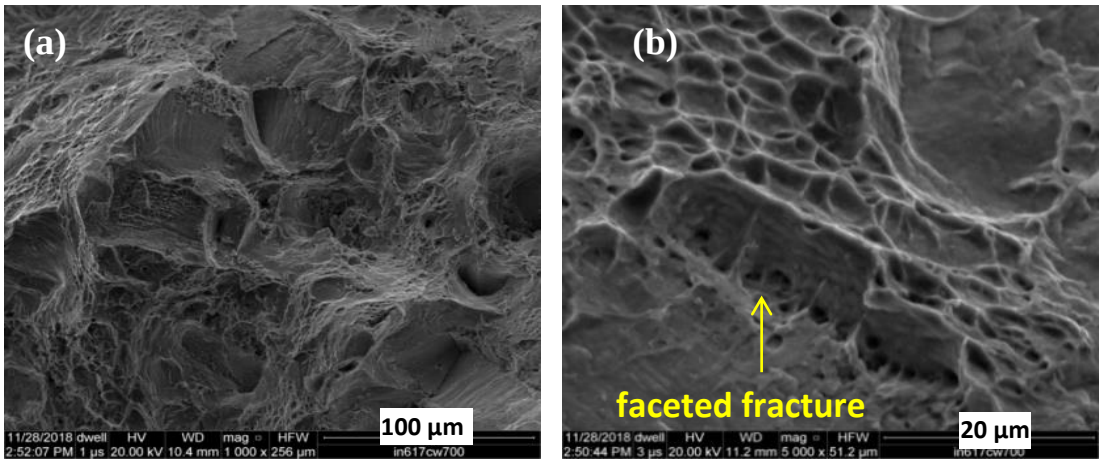

Fig. 4.16: SEM fractographs of tensile tested samples at 700^{o}C in SQ-CW condition showing: (a) dimples with cleavage facets and (b) magnified view of the facets.

4.8 Discussion

4.8.1 Engineering Stress-Strain Behaviour

Grain size, prior dislocation density, precipitates and stacking fault energy (SFE) are the four main factors that control mechanical properties of the material. The grain size of the SQ, SQ-AG1 and SQ-AG-2 conditions is nearly same however the dislocation density would be relatively less in the aged samples. Hence, the increase in the strength of the SQ-AG1 and SQ-AG2 conditions can be attributed to the carbide precipitates formed due to aging. Strengthening of the SQ-CW samples at RT is essentially due to very high dislocation density and formation of strong barriers resulting from the interaction of gliding dislocations in different slip bands during the process of cold rolling. The coarse grain size in the SQ, SQ-AG1 and SQ-AG2 conditions facilitated smooth glide of dislocations because of less hindrance from grain boundaries which contributed to high ductility in these samples. The marked increase in the yield strength, close to UTS, caused drastic reduction in the both uniform (e_{pu}) as well as total elongation (e_{pf}) in the SQ-CW sample. The intergranular coarse carbides

present in the SQ condition, got elongated in the rolling direction and some of them were cracked during the cold working. Uniform elongation is a very important factor for mechanical processing and design of structural components. Uniform elongation in the SQ condition is higher than the other conditions at both RT and 700^{o}C. At 700^{o}C, the SQ-CW material showed very high strength, more than three times of the SQ, because there was no recrystallization of the deformed matrix as the recrystallization temperature was higher than 700^{o}C [53, 54].

The higher S_{UTS}/S_{YS} ratio in the SQ condition at RT is due to coarse grains, due to which gliding of dislocations was relatively easier, because of the less number of grain boundary barriers. At 700^{o}C, the highest degree of work hardening in the SQ-AG2 condition may be attributed to formation of additional precipitate during the process of tensile loading. The precipitation of carbides and γ′ and their interaction with dislocations during tensile loading contributed to higher degree of work hardening (S_{UTS}/S_{YS}) at 700^{o}C compared to that of RT in all the conditions.

4.8.2 Work Hardening Behaviour

It has been observed in the low SFE metals and alloys that as the strain increases the deformation mode gradually changes from planar slip to cross slip [103] and Inconel 617 alloy is considered a low stacking fault energy material [56]. Climb and cross slip are difficult in these alloys in the low strain range due to low SFE, consequently the flow stress and θ are increased markedly. The increase in the dislocation density in the planar slip bands caused by pile-up at grain boundary leads to high θ in the initial stage, thus in the low strain region the double logarithmic plot between true stress- true plastic strain progressively displayed upward concave shape (Fig. 4.6). This typical behaviour has been reported by several researchers for the fcc materials such as nickel based

superalloys and austenitic stainless steels [103-106]. The decrease in the strength coefficient (K) at 700^{o}C is due to dynamic recovery. K value for the SQ-CW condition at 700^{o}C is high due to the synergistic effect of pre-existing high dislocation density and precipitates in this condition. K_1 corresponds to short range stresses inducing the movement of first mobile dislocations whereas the $-n_1$ expresses the rate of decrease in the ratio between the short range stresses and the long range stresses, with increase in the plastic strain [106].

Generation of dislocations, their arrangement, annihilation, precipitation of particles and the interaction of precipitates with dislocations affect hardening/dynamic recovery of metallic materials. The high value of θ in the initial stage with the commencement of plastic deformation can be attributed to accumulation of dislocations at barriers and their multiplication. The pre-existing high dislocation density in the SQ-CW condition of the alloy contributed to the high initial rate of work hardening. Further increase in the stress led to annihilation of the dislocations which decreased the value of θ. Buildup of back stress at the grain boundaries and carbides increased θ in the early stage of inelastic deformation. During tensile loading, at higher strains where multiple slip systems are activated and more homogenous dislocation substructure is formed, the work hardening rate decreases.

It may be seen from Fig. 4.8 that, while there are three stages in the plot of θ *vs.* σ in the three conditions (SQ, SQ-AG1 and SQ-AG2), in contrast, there is only stage I in the SQ-CW condition both at RT as well as 700^{o}C. This is an interesting observation related to the effect of cold working on the variation of θ with σ displaying only stage I. Further, the rate of fall in θ with stress is most rapid in the cold worked condition. The rapid drop in θ can be attributed to pile up of dislocations which cause saturation of the plastic strain rate, as observed in several *fcc* materials [102-106]. The absence of stage

II and III in the SQ-CW condition may be attributed to very low uniform deformation and consequent early necking in the material. Stage I is associated with elasto-plastic transition. The slope of the line in the stage II (incubation stage), is comparable in the three conditions, it is relatively higher in the SQ at RT. Thus, it is obvious that it is independent of temperature (athermal), as also observed by Venkadesan et al. [107] in the austenitic stainless steels. Due to dynamic recovery, the deviation from the straight line behaviour at the end of stage II, started at lower stress range for 700^{o}C compared with that at RT (Fig. 4.8). The critical stress (σ_c), at the end of stage II also decreased with increase in temperature due to climb and slip of dislocations. The Stage III is associated with dynamic recovery and increment of localized stresses which increased the tendency to cross slip and reduced the work hardening rate [56].

4.8.3 Deformation Behaviour

The arrangement of dislocations and their mutual interaction varies in different conditions of the material and with the test temperature. At RT, slip is the primary mode of deformation in the SQ condition, as evidenced by the traces of slip bands. Interaction of precipitates and dislocations in this condition is not observed at this temperature. Deformation mechanism in the aged condition is similar to that of the SQ due to comparable microstructure, except the presence of few precipitates and their interaction with dislocations which resulted in increase of strength. Similar observations have been made by several researchers for the same duration of aging at varying temperatures [14, 51].

At 700^{o}C, twinning is the main mode of deformation in all the conditions. Initially deformation takes place by planar slip and is followed by twinning at higher strains as observed in the Nb-Ti stabilized IF steel [108]. Two stage of deformation is

also supported by the sudden drop in θ in the initial stage, followed by stable region of stage II with increase in σ (Fig. 4.8). This is associated with smooth process of slip till it reaches the saturation state. Formation of fine precipitates of carbides and γ' and their interaction with dislocations is the prime cause of strengthening and work hardening of the Inconel 617 alloy at 700^{o}C.

4.8.4 Fracture Behaviour

Ductile fracture with micro void coalescence occurred at room temperature in the SQ condition owing to the fact that grain boundary strength is high and deformation was concentrated within the grains. Growth and coalescence of these voids finally led to ductile fracture with dimples. The fracture mode of the aged specimens is similar to that of the SQ condition, except that the fine dimples in between the facets are comparatively more in number in the aged condition. A careful examination of the facets on fracture surface of the SQ-CW sample reveals ripple marks, resulting from progressive propagation of the cracks, initiated from the grain boundaries due to breaking and de-cohesion of the coarse carbides along the grain boundaries. The growth and linkage of the cracks led to formation of intergranular cracks during tensile testing. The process of intergranular cracking reduced the effective load bearing cross sectional area during tensile testing and gave rise to early necking. The stress in the necked region progressively increased with necking and the intergranular cracks propagated as revealed by the ripples on the facets.

Though the mode of fracture at both the temperatures was similar with dimples, however, the size of the dimples was larger in the samples tested at 700^{o}C due to increased plasticity of the material. Same features were observed in the samples of all the other conditions tested at 700^{o}C, with only a slight variation in the number of the

facets and their configuration. On the other hand, there was nominal improvement in the ductility of the cold worked material at 700^{o}C as compared to that at RT. It was due to the initial damage in the grain boundaries due to cracking and de-cohesion of the coarse carbides associated with grain boundaries, during the cold rolling at RT. Therefore, during tensile testing even at 700^{o}C there was not much improvement in ductility because of growth and linkage of the cracks formed due to cold rolling, during tensile testing at 700^{o}C.

4.9 Chapter Summary

A detailed study was carried out on tensile plastic flow behaviour of the Inconel 617 alloy, a promising material for advanced ultra-super critical power plants (A-USC), in four conditions (SQ, SQ-AG1, SQ-AG2 and SQ-CW) at RT and at the service temperature of 700^{o}C. The following important findings can be summarized from the analysis.

1. There was best combination of strength and ductility in the SQ condition, with coarse grained microstructure both at RT as well as 700^{o}C. Marginal reduction in ductility was observed in this condition at 700^{o}C due to precipitation of carbides. The YS and UTS were increased and ductility was reduced at RT, due to the aging treatment (SQ-AG1 and SQ-AG2). However, there was not any appreciable difference in the strength and ductility with increase in the duration of aging.
2. There was marked improvement in the YS of the cold worked material both at RT and 700^{o}C, in respect of the SQ, SQ-AG1and SQ-AG2 conditions, but the ductility parameters, in particular the uniform elongation was drastically reduced. Uniform elongation is an important factor for mechanical processing

and design of structural components. It will be useful to study the effect of varying degree of cold working and aging at elevated temperatures to achieve a better combination of strength and ductility both at RT and 700^{o}C.

3. Among the five relationships proposed for the characterization of work hardening parameters of metallic materials, the one proposed by Ludwigson was found to fit the best with the experimental data.
4. While there were three stages in variation of θ with stress (σ) both at RT and 700^{o}C in the three conditions (SQ, SQ-AG1 and SQ-AG2), there was only stage I in the SQ-CW condition at RT and 700^{o}C. Further, the rate of fall in θ in the cold worked condition is much higher than in the other three conditions.
5. Slip was observed as dominant process of plastic deformation at RT whereas both slip and twinning were operative at 700^{o}C. The interaction of dislocations with carbides and γ' precipitates, leading to high work hardening at 700^{o}C was clearly established through the transmission electron microscopy.
6. Fracture surfaces resulting from testing at RT and 700^{o}C revealed dimples of varying sizes in the different conditions. There were facets on fracture surface of the cold worked material tested both at RT as well as 700^{o}C, resulting from cracking/de-cohesion of carbides at grain boundaries due to 40% cold reduction, therefore there was no improvement in ductility at 700^{o}C.